




Article

Experimental Study of Advanced Helmholtz Resonator Liners with Increased Acoustic Performance by Utilising Material Damping Effects

Martin Dannemann ^{1,*}, Michael Kucher ¹, Eckart Kunze ¹, Niels Modler ¹,
Karsten Knobloch ², Lars Enghardt ², Ennes Sarradj ³ and Klaus Höschler ⁴

¹ Institute of Lightweight Engineering and Polymer Technology (ILK), Technische Universität Dresden, Holbeinstraße 3, 01307 Dresden, Germany; michael.kucher@tu-dresden.de (M.K.); eckart.kunze@tu-dresden.de (E.K.); niels.modler@tu-dresden.de (N.M.)

² German Aerospace Center (DLR), Institute of Propulsion Technology, Engine Acoustics, Müller-Breslau-Str. 8, 10623 Berlin, Germany; karsten.knobloch@dlr.de (K.K.); lars.enghardt@dlr.de (L.E.)

³ Institute of Fluid Mechanics and Engineering Acoustics, Technische Universität Berlin, Einsteinufer 25, 10587 Berlin, Germany; ennes.sarradj@tu-berlin.de

⁴ Chair of Aircraft Engine Design, Brandenburg University of Technology Cottbus-Senftenberg, Siemens-Halske-Ring 14, 03046 Cottbus, Germany; klaus.hoeschler@b-tu.de

* Correspondence: martin.dannemann@tu-dresden.de; Tel.: +49-351-4633-8134

Received: 27 September 2018; Accepted: 10 October 2018; Published: 15 October 2018



Abstract: In aero engines, noise absorption is realised by acoustic liners, e.g., Helmholtz resonator (HR) liners, which often absorb sound only in a narrow frequency range. Due to developments of new engine generations, an improvement of overall acoustic damping performance and in particular more broadband noise absorption is required. In this paper, a new approach to increase the bandwidth of noise absorption for HR liners is presented. By replacing rigid cell walls in the liner's honeycomb core structure by flexible polymer films, additional acoustic energy is dissipated. A manufacturing technology for square honeycomb cores with partially flexible walls is described. Samples with different flexible wall materials were fabricated and tested. The acoustic measurements show more broadband sound absorption compared to a reference liner with rigid walls due to acoustic-structural interaction. Manufacturing-related parameters are found to have a strong influence on the resulting vibration behaviour of the polymer films, and therefore on the acoustic performance. For future use, detailed investigations to ensure the liner segments compliance with technical, environmental, and life-cycle requirements are needed. However, the results of this study show the potential of this novel liner concept for noise reduction in future aero-engines.

Keywords: acoustic liner; broadband noise; Helmholtz resonator; honeycomb sandwich panel

1. Introduction

Acoustic liners are used for dissipation of aero-engine noise, for instance in the intake and bypass ducts of aircraft engines. Basically, conventional aircraft liners convert acoustic energy to turbulent fluid motion and thermal energy due to the induced periodic in and outflow as well as viscous effects. Helmholtz resonators (HR) efficiently reduce propagating noise at their resonance frequencies and depict a simple construction requiring only small assembly space [1]. Single-Degree-of-Freedom (SDOF) liners consist of a perforated face sheet covering a series of small cavities [1] and a rigid back layer (Figure 1a).

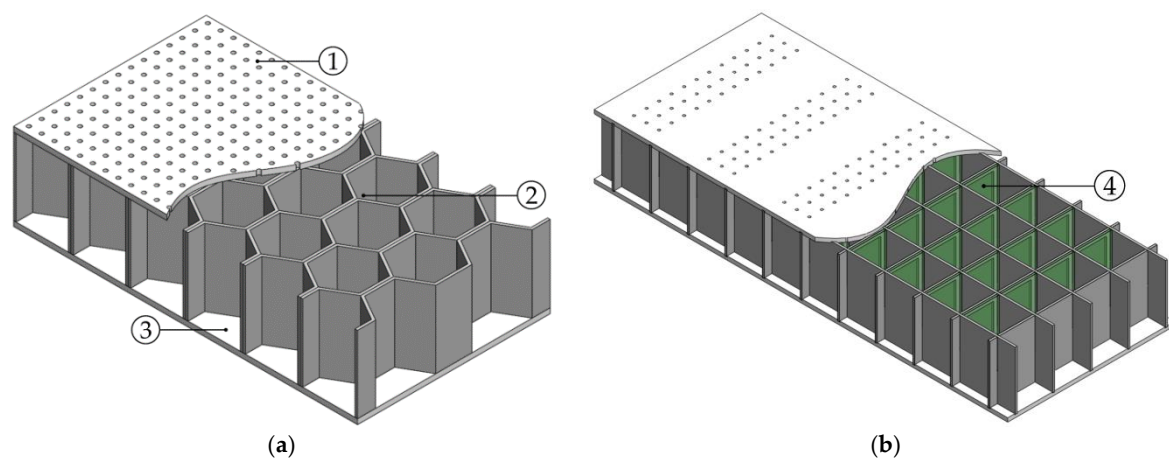


Figure 1. (a) Conventional acoustic liner with hexagonal honeycomb structure consisting of perforated face sheet, 1, hexagonal honeycomb core, 2, and, a back plate, 3; (b) novel liner concept with partially flexible walls, 4.

By varying the porosity, the thickness of the face sheet, or the cavity dimensions the sound attenuation properties can be tuned [1]. Several studies exist addressing damping of acoustic liners [2]. Conventional acoustic liners have the main disadvantage of fixed, rather narrow absorption peaks due to their geometry. However during different flight phases—corresponding to varying engine operating conditions, such as take-off, cut-back, and approach- the required frequency of maximum absorption (e.g., the first and second blade passing frequency) will change. There are several concepts to improve sound absorption and obtain more broadband noise absorption. One promising approach is to use multilayer HR liner, so-called double- or multiple-degree-of-freedom (DDOF/MDOF) liners [3]. This kind of resonators usually require more installation space that is not available for flow-optimised engine nacelles, as well as more challenging fabrication technology, due to their multi-layer construction. For SDOF liners different concepts for tuneable HR-structures can be found in literature [4]. One approach is the adjustment of the cross-sectional area A_L of the perforation [5–7], another the change of the cavity's volume [8–10], a combination of both or the change of the neck length l_H . All active geometry adjustment approaches are technologically difficult to implement due to size, weight, and reliability issues [4]. In addition to these geometric adjustments, the usage of active sound absorbing structures, such as HRs with a compliant piezoelectric composite back-plate [11,12] or HRs with movable walls [13] comprise the possibility to shift the resonant frequencies and tune the impedance.

Another promising approach is the combination of conventional HR liners with other noise absorbing structures. Studies by Knobloch et al. [14] and Höschler et al. [15] show that the partial replacement of rigid resonator cell walls by flexible walls with intrinsic damping has a positive effect on sound absorption of acoustic liners. The resulting structure is sketched in Figure 1b. Due to the acoustic-structural interaction inside the cells, the overall damping performance is enhanced. In this realization, one or more walls of the honeycomb structure have rectangular cut-outs which are covered by highly-flexible films made of thermoplastic polymers. It is assumed that the mechanism responsible for the improved sound absorption by the flexible cavity walls is similar to the working principle of panel sound absorbers [16,17]. The liners are called FlexiS (flexible structure) liner.

For the validation of the FlexiS liner concept, samples have been build that are investigated in a flow duct with plane acoustic wave excitation. Thus the flexible walls were perpendicular to the main flow direction and the cell walls in mean flow direction were kept rigid to ensure structural strength.

For the manufacturing of the honeycomb-like core structure used in conventional aero engine liners, different materials and technologies are used. Depending on the service temperature, honeycombs are made of aluminium, stainless steel or FRP [18]. Components of FRP can be aramid fibre, glass fibre or cellulose fibre as reinforcement and phenol resin or polyimide as matrix material.

Common core structures have a cell size of 1/8" (3.175 mm) to 1" (25.4 mm) [18,19]. Especially in low temperature regions, such as the bypass area, epoxy-based FRP top layers and core structure are used [20]. Typically a unit cell of the core structure has a prismatic cellular structure with a triangular, square or hexagonal shape. For a long time, liners were manufactured in sections and installed inside the nacelle [21]. This resulted in liner splices between the acoustic liner segments, which causes acoustic scattering due to discontinuities in the acoustic impedance around the circumference of the duct [21]. Therefore, latest developments include spliceless liner barrels, which are far more expensive and difficult to handle for assembly and maintenance.

Depending on the raw material and the desired geometry different manufacturing methods are available to realise the segmented acoustic liner [22,23]. Wadley [22] described, inter alia, an expansion manufacturing process, a corrugation manufacturing process and a strip slotting method. Most honeycombs are fabricated by the expansion process. Thereby thin metal or paper sheets are laser welded or adhesive bonded to Hobe blocks, respectively [22,24]. These blocks are cut and afterwards stretched to create hexagonal structures or over expanded to form rectangular structures. To enable sheet stretching, a moderately high inter sheet bond strength is required. Thus, this manufacturing process is only suitable for thin-walled semi-finished products. For honeycombs made of stainless steel sheets, the corrugation process is used. The sheets are corrugated by rolls or a press and stacked [22]. The layers are welded or adhesively bonded together. The strip slotting method is used for square and triangular honeycombs of non-ductile materials such as ceramics [22,25]. The strips are bonded by means of adhesives or by brazing. The installation effort increases significantly with increasing number of connections between strips which makes the process primarily suitable for small quantities of honeycombs. However, the strip slotting method enables the manual production of arbitrary honeycomb wall structures and is used in this study to fabricate the core structure with partially flexible walls.

In this study a new design of a HR liner with partially flexible walls is investigated using different materials as flexible walls. An approach for the manufacturing of this novel acoustic liner and the determination of acoustical and structural properties is described. The acoustic damping characteristics of all manufactured liner samples and the deformation behaviour of the square honeycomb core structure is investigated. Furthermore, the influence of the applied fabrication technology and the production-related manufacturing tolerances is analysed. A comprehensive assessment of the properties and implications of this novel acoustic liner is made with respect to designated future aircraft application.

2. Acoustic Liner Design

2.1. Resonator Design

The basic setup of the liner samples with flexible structures (FlexiS liners) investigated in the framework of this study is comparable to conventional HR liners (SDOF liner). The desired plane wave excitation regime inside the flow duct and the duct dimensions determine the cell size and the perforation of the face sheet. The acoustic damping of the resonator has its maximum at the cavity's resonance frequency. This can be estimated by the Helmholtz equation:

$$f_H = \frac{c_0}{2\pi} \sqrt{\frac{A_L}{V_C(h_L + \pi d_L)}} \quad (1)$$

where c_0 is the speed of sound, A_L the open area of the perforation, V_C the volume of the cavity, h_L the height of the perforation hole and d_L its diameter (Figure 2a).

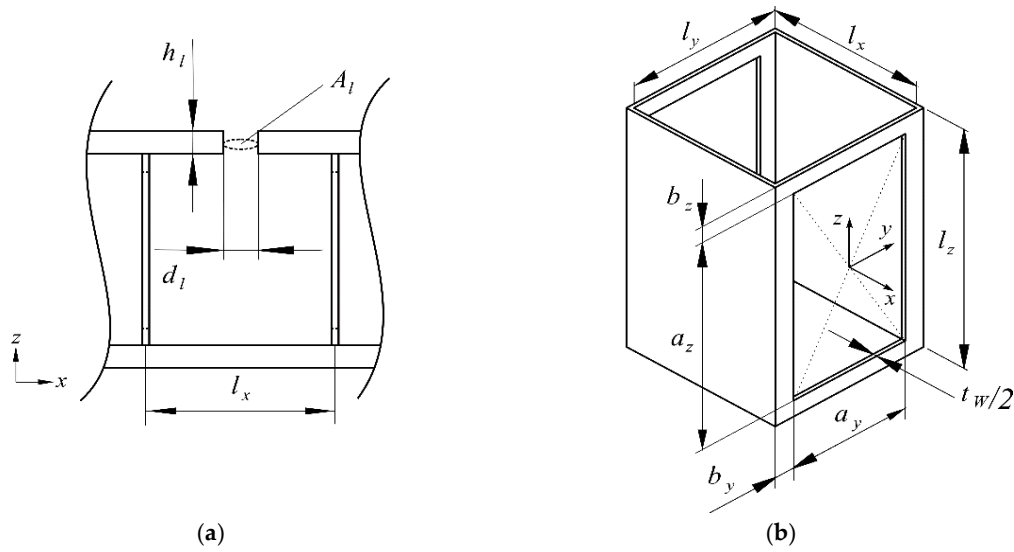


Figure 2. Unit cell of support structure square honeycomb (with cut-outs for flexible walls): (a) cross section view with face sheet and back plate; (b) three-dimensional view of square honeycomb unit cell.

A second damping maximum is observed for frequencies with a wavelength equal to one quarter of the resonator depth (resulting in destructive interference of the incident and the reflected acoustic wave). In order to separate both phenomena, the cavity size was chosen 19 mm by 19 mm in length l_x and width l_y and 30 mm in depth l_z . This results in $V_C = 10.8 \text{ cm}^3$ of the honeycomb structure's cavities. The upper boundary of the cell consists of a perforated plate with 9 holes of diameter 1.3 mm covering each cell, while the lower cell wall is stiff (Figure 3). Thereby, the Helmholtz resonance occurs around 1040 Hz, while the quarter wave resonance occurs around 2860 Hz.

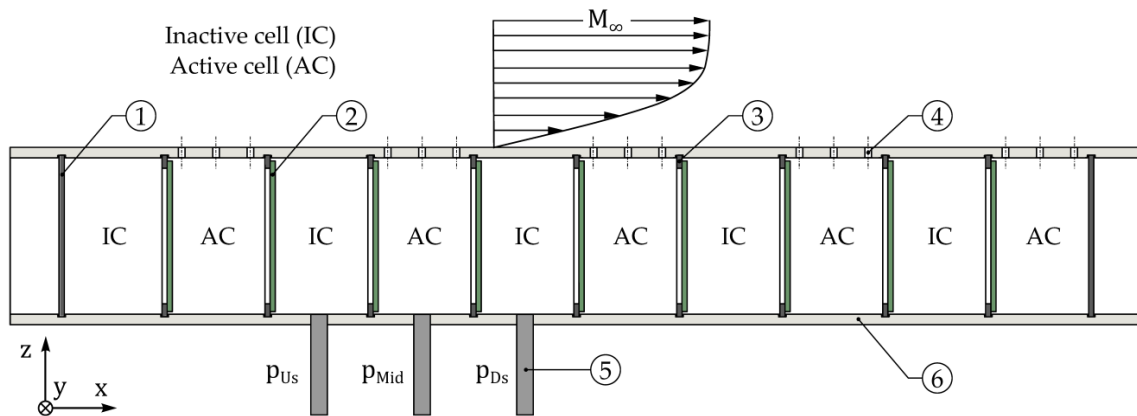


Figure 3. Schematic of acoustic liner sample with rigid external walls, 1, polymer films, 2, walls with cut-outs, 3, face sheet with perforations, 4, optional in-cell microphones, 5 and back layer, 6.

2.2. Structural Design of Resonator Cell

Each sample consists of 10 by 4 square cavities, ten in main flow (x -) direction and four in spanwise (y -) direction, respectively (Figure 1b). All liners have exactly the same cell dimensions and share the same cover and back layer design. The internal cell walls in spanwise direction were covered with polymer film. Thus, the support structure of each unit cell of the honeycomb core contains two solid walls and two cut-out walls (Figure 2). The polymer films are adhesive bonded to the cut-out

walls. Depending on the dimensions of the unit cell the relative density of the support structure can be obtained by

$$\bar{\rho} = \frac{\rho}{\rho_s} = \frac{(l_x + l_y + t_W)t_W}{(l_x + t)(l_y + t)} - \frac{n(l_y - 2b_y)(l_z - 2b_z)t_W}{2(l_x + t)(l_y + t)l_z} \quad (2)$$

where ρ is the density of the cellular structure, ρ_s is the density of the material of the support structure and n is the number of cut-outs, which is $n = 2$ in this study.

In order to enable the deflection of the flexible walls, between the active cells some inactive volume was placed between a pair of cells in the direction of the grazing sound field—which is identical with the main flow direction (Figure 3). The face sheet of each second row in main flow direction (containing the active cells—AC) is provided with the 3 by 3 perforations described above. The intermediate rows (inactive cells—IC) only have integrated pressure compensation holes. The liners' outer dimensions in spanwise and main flow direction were chosen to fit the acoustic testing rig. The liner height was comparable to conventional acoustic liners.

2.3. Vibration Design of Flexible Walls

Analogously to a panel sound absorber, it is assumed that flexible walls inside each cavity improve the sound absorption of the acoustic liner due to the acoustic-structural interaction. Therefore, one or more walls of the honeycomb structure comprise rectangular cut-outs which are covered by flexible polymer films that exhibit significant material intrinsic damping (see Table 1).

Table 1. Properties of polymer films under standard atmospheric conditions (i.e., 23 °C, 50% relative humidity).

Properties	Unit	TPU 1170 A	TPU 1195 A
Density ρ	g/cm ³	1.08 [26]	1.15 [26]
Young's modulus	MPa	16 ¹ [27]	91 ¹ [28]
Mechanical loss coefficient $\tan \delta$	-	0.05 [27]	0.13 [28]
Poisson's ratio	-	0.48 [29]	0.48 [29]
Moisture absorption	%	0.5 * [30]	0.4 ... 0.7 [29]
Nominal thickness t_F	mm	0.3	0.1, 0.5

¹ Calculated with dynamic shear storage modulus, * Material property of TPU 1175 A.

To approximate the damping characteristic of the novel HR liner concept, the flexible walls inside each cavity are considered as free plates without considering the impedances of the enclosed air volume. The films were modelled as three-dimensionally deformable body clamped at all sides. The size of the flexible walls is restricted by the size of the liner cavities (Figure 2b). To ensure a reliable bonding of the polymer films, sufficient adhesive surface is needed. The frame width on each side of the cut-out was $b_y = b_z = 2$ mm, which leads to cut-out with the dimension $a_y = 15$ mm and $a_z = 26$ mm. These lengths represent the size of the freely vibrating flexible wall. For the calculation of the eigenfrequencies, constant elastic properties and material damping of the polymer films are assumed (Table 1). For the investigation of the influence of the pre-stress, numerical modal analysis of the film's vibration behaviour was calculated by using the finite element method. Linear brick elements with reduced integration were used for discretisation. Linear mesh convergence studies (not reported here) have been done and indicate that the used mesh size yields acceptably accurate results for most of the values of interest. The film's sides were fixed in all directions.

The coordinate system—which is used to describe the lateral deflection of the flexible wall—is depicted in Figure 2. The axes are parallel to the sides a_y and a_z of the cut-outs. The frequencies' modes m and n are associated to the y - and z -direction. To model the pre-stress of the flexible films, an additional load resulting in a constant deformation in y -direction was included. With an increasing uniaxial stress state the film thickness decreases due transversal contraction. The resulting modal

analysis shows increasing natural frequencies with an increasing pre-stress (Figure 4). The design point for the acoustic flow duct is the first eigenfrequency f_{11} , which must be in the range up to 2000 Hz. The number of natural frequencies in the relevant range is very low for the sample 1195 A, $t_F = 0.5$ mm, which indicates that film press stress is relevant (Figure 4).

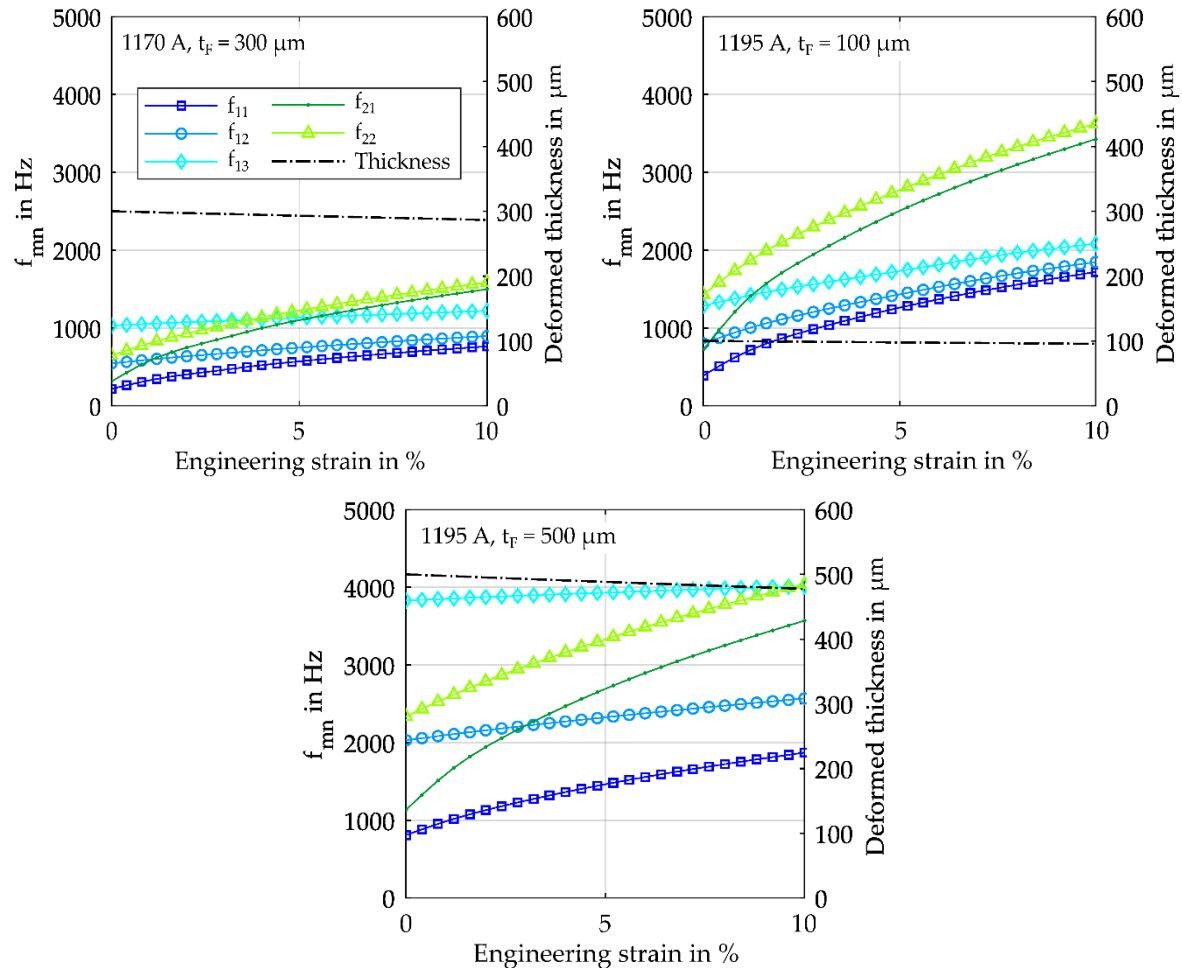


Figure 4. Numerical analysed influence of pre-stress on the vibration behaviour of polymer films.

3. Materials and Fabrication

3.1. Honeycomb Core Materials

The new concept of acoustic liner consists of rigid and flexible wall areas. To ensure a high resistance against compression of the core structure, the partially flexible walls are realised by cut-outs of the rigid walls. The walls representing the support structure of the core were made of aluminium ALMG3 H22. Several thin films materials with high intrinsic material damping, which are applied upon the edge area of the cut-out wall segments, are available. The films were made of conventional thermoplastic polyurethane (TPU) from BASF. The material was selected due to its high damping properties and a high resistance to oils, greases, oxygen and ozone [26]. Two TPUs with different elasticity and damping properties in different thicknesses were chosen for the flexible walls (Table 1). In this study thin films were used to ensure a maximal acoustic-structural interaction and thus a higher dissipation of acoustical energy.

The flexible films were cut out from TPU material, which comes rolled up. A measurement of the roll's thickness in width direction shows that the thickness varies. It has its highest value in the edge

regions of the film (Figure 5). The film material used for the flexible walls was cut from the middle section of the basic material due to the non-constant thickness of the films.

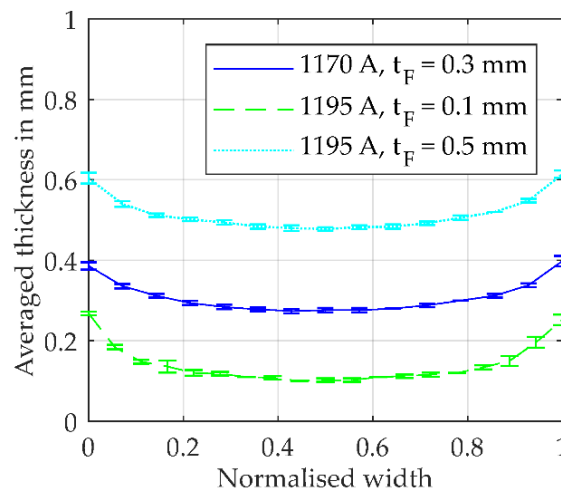


Figure 5. Manufacturing-related thickness variation of TPU films (semi-finished product, full width) and its standard deviation.

3.2. Fabrication and Assembly of Novel HR Liner

The honeycomb structures in this study were manufactured using the strip slotting method. For the fabrication of the walls a laser cutting process was used to fulfil the high accuracy requirements. To improve the adhesive strength the bonding surfaces were sanded. The films were bonded to the walls with cut-outs using epoxy resin. Each film was fixed without stress. After adhesive bonding, the strips were assembled. The resulting core structure was glued to the top and bottom layers using epoxy resin. Grooves enabled an accurate positioning and angularity of the acoustic liner. During the bonding process it was ensured that none of the perforations were closed (Figure 6).

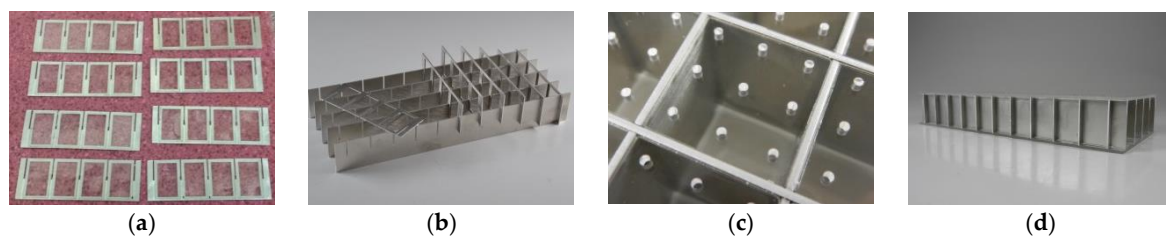


Figure 6. Manufacturing of acoustic liner samples: (a) adhesive bonding of films; (b) assembling of support structure; (c) attachment of face sheet; (d) acoustic liner sample.

Using this approach three liners with partially flexible walls were built (Table 2). For reference, an identical sample with rigid internal cell walls (called reference liner) was manufactured and tested under the same conditions as the FlexiS liners.

Table 2. Investigated acoustic liner configuration.

Liner	TPU Film	Nominal Thickness t_F in mm	Number of Flexible Walls Per Cavity
1170 A, 0.3 mm	1170 A	0.3	2
1195 A, 0.1 mm	1195 A	0.1	2
1195 A, 0.5 mm	1195 A	0.5	2
Reference	-	-	0

4. Acoustic Testing and Results

4.1. Experimental Setup, Data Acquisition and Processing

In order to assess the acoustic performance of the liner samples, measurements were conducted in the test section of the DUCT aCOustic Test rig- Rectangular cross section (DUCT-R) facility of the German Aerospace Centre (DLR) in Berlin. The test rig has a length of about 8 m and consists of two symmetrical sections; each containing several microphones and a loudspeaker for acoustic excitation (see sketch in Figure 7). The cross section of the rig was 60 mm × 80 mm.

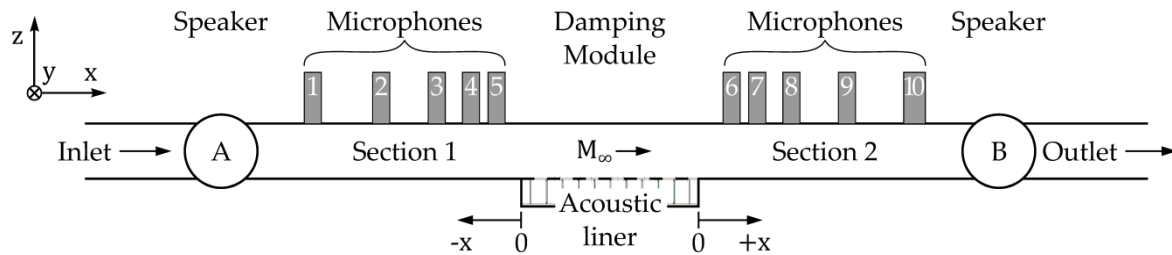


Figure 7. Sketch of acoustic test rig DUCT-R.

A radial compressor was connected to the upstream part of the duct and provides a grazing flow across the test object with a maximum Mach number of 0.3 at the duct centreline. The rig has been used extensively during the last years for the investigation of acoustic scattering coefficients and impedances of several liner types.

The basic setup for the acoustic measurements is identical to the setup for a conventional single-degree-of-freedom (SDOF) liner. Consecutively, six multi-tones are excited and fed into the rig by either the upstream or the downstream speakers. Thereby, a frequency range from 204 to 2091 Hz with 51 Hz resolution is covered. The overall sound pressure level (SPL) of these multi-tones was adjusted to about 130 dB in maximum, but this could not be fully ensured for all frequencies due to the coupling of the speaker driver and the speaker characteristics. The acoustic investigation was limited to the plane wave regime (cut-on frequency for higher-order modes is about 2150 Hz for the no-flow case). For each liner test configuration, two different sound fields are excited consecutively in two separate measurements. Speaker A is used in the first measurement and in the second measurement the same signal is fed into speaker B.

Then, the data of Sections 1 and 2 (index 1 and 2) are analysed separately. Thereby, the sound field is decomposed into upstream and downstream traveling waves and their respective complex sound pressure amplitudes for each section and measurement. By a combination of all measurements, the influence of end reflections can be cancelled out, and the reflection coefficient r and transmission coefficient t for the acoustic pressure can be calculated.

The energetic quantities are obtained applying the acoustic energy flux in a moving medium as given by Blokhintsev [31]. After integrating over the duct cross section A , this yields for the power of the downstream traveling wave P^+ , respectively the upstream traveling wave P^- :

$$P^\pm = \frac{A}{2\rho c} (1 \pm M)^2 |p^\pm|^2 \quad (3)$$

where M is the mean Mach number of the flow, ρ the density, c the speed of sound, and p^\pm the complex pressure amplitude of the downstream/upstream traveling wave. Then, the energy coefficients for reflection R^\pm and transmission T^\pm can be given relative to the pressure coefficients. The dissipation of acoustic energy is expressed by the dissipation coefficient Δ^\pm . The dissipation coefficient can be calculated directly from the reflection and transmission coefficients via an energy balance:

$$R^\pm + T^\pm + \Delta^\pm = 1 \quad (4)$$

The energy of the incident wave is partly reflected, partly transmitted, and partly dissipated inside the damping module. R and T are the power quantities of the reflection and transmission coefficients, while r and t denoted the pressure quantities. Assuming the same flow conditions and cross-sectional area in Sections 1 and 2, finally, the dissipation coefficients of the test object for the downstream Δ^+ and upstream direction Δ^- can be obtained:

$$\Delta^\pm = 1 - \frac{(1 \mp M)^2}{(1 \pm M)^2} |r^\pm|^2 + |t^\pm|^2 \quad (5)$$

This is an integral value of the acoustic energy that is absorbed while a sound wave is passing the damping module. The dissipation coefficient is used to evaluate the damping performance of the test object, here the FlexiS liner. For most comparisons, the averaged value $\Delta_{avg} = \Delta^+ / 2 + \Delta^- / 2$ can be used.

For each liner (3 FlexiS liner and one reference liner), measurements were made for 120 dB and 130 dB overall SPL. The Mach number was varied between $M = 0$ (no-flow case), $M = 0.1$, and $M = 0.2$. These values always mark the center-line Mach number. In this paper, only data for the 130 dB excitation is presented.

Although the flexible cell walls are not directly accessible inside the assembled liner samples, some tests were made in order to investigate the movement and effect of the flexible structures. Therefore, a specific sample with four cut-outs and TPU film was prepared. This sample represents a single wall segment with cut outs and was installed between the two microphone sections of the DUCT-R instead of the liner damping module. Only no-flow measurements could be made in this configuration, because this specific sample represents a partition wall in the duct.

Finally, three microphones were mounted flush with the inside of the back plate of three neighbouring liner cells- aligned along the main flow axis (Figure 3). Thereby, the pressure p_{Us} upstream, p_{Ds} downstream and p_{Mid} at these positions and the phase relation between active cells and inactive cells could be determined.

4.2. Damping Performance of Acoustic Liner

Figure 8 shows the comparison of the averaged dissipation coefficients for the no-flow case ($M = 0$). The reference HR liner with rigid walls (reference liner) was prepared the same with alternating active and inactive cell rows in main flow direction.

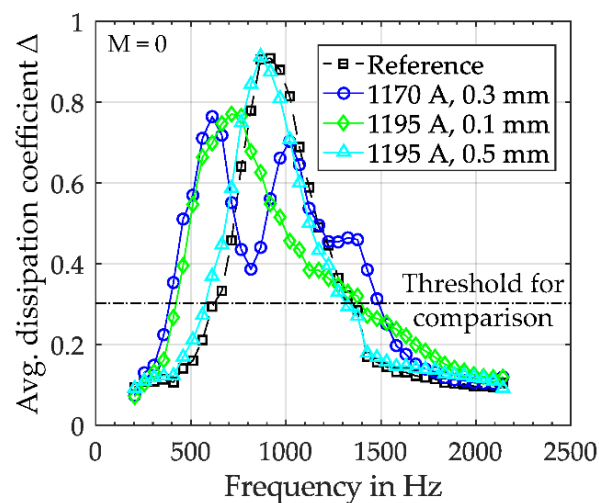


Figure 8. Comparison of the averaged dissipation coefficients for the no flow case ($M = 0$).

Most of the FlexiS configurations demonstrate a significant increase of the dissipation in the frequency range from 400 to 800 Hz. The material 1170 A, 0.3 mm shows even three local dissipation

maxima at 600, 1000 and 1350 Hz. However, the widening of the bandwidth goes along with a reduction in peak performance compared to the reference liner. The dissipation maximum of the sample with the 1195 A, 0.1 mm material is shifted from 940 Hz (Reference) to around 750 Hz.

In Table 3, the benefit is quantified by introducing an artificial threshold ($\Delta > 0.3$) for which the lower and upper frequency limits are given. Furthermore, the area between the threshold and the damping curve is compared to the reference liner. A significant increase in the frequency range, a shift towards lower frequencies, and an increase of “integral” damping is observed for three FlexiS liners (1170 A, 0.3 mm, 1195 A, 0.1 mm). The 1195 A, 0.5 mm liner exhibits only a small shift towards lower frequencies, but does not yield additional benefits. In the case with grazing flow (not shown here) the observed behaviour holds with improved acoustic damping for the FlexiS liner.

Table 3. Comparison of damping curves (only dissipation data above $\Delta = 0.3$ is considered here).

Liner	f_{low} (Hz)	f_{high} (Hz)	“Dissipation Increase” to Ref.
1170 A, 0.3 mm	387	1490	+31%
1195 A, 0.1 mm	421	1398	+14%
1195 A, 0.5 mm	576	1317	−0.3%
Reference	617	1355	0

4.3. Vibrations of Acoustic Excited Polymer Films

A more detailed characterisation of the flexible material was the aim of the investigation with isolated flexible structures. The results (only no-flow measurements possible) are shown in Figure 9. It can be assumed that the acoustic excitation of the flexible structure from one side propagates best to the other side of the facility, if the structure is deflected/vibrating. Therefore, an increase in transmission (green curves with diamonds) relates to a vibrating flexible structure. In addition, the material-inherent damping should be most effective, if the structure is vibrating.

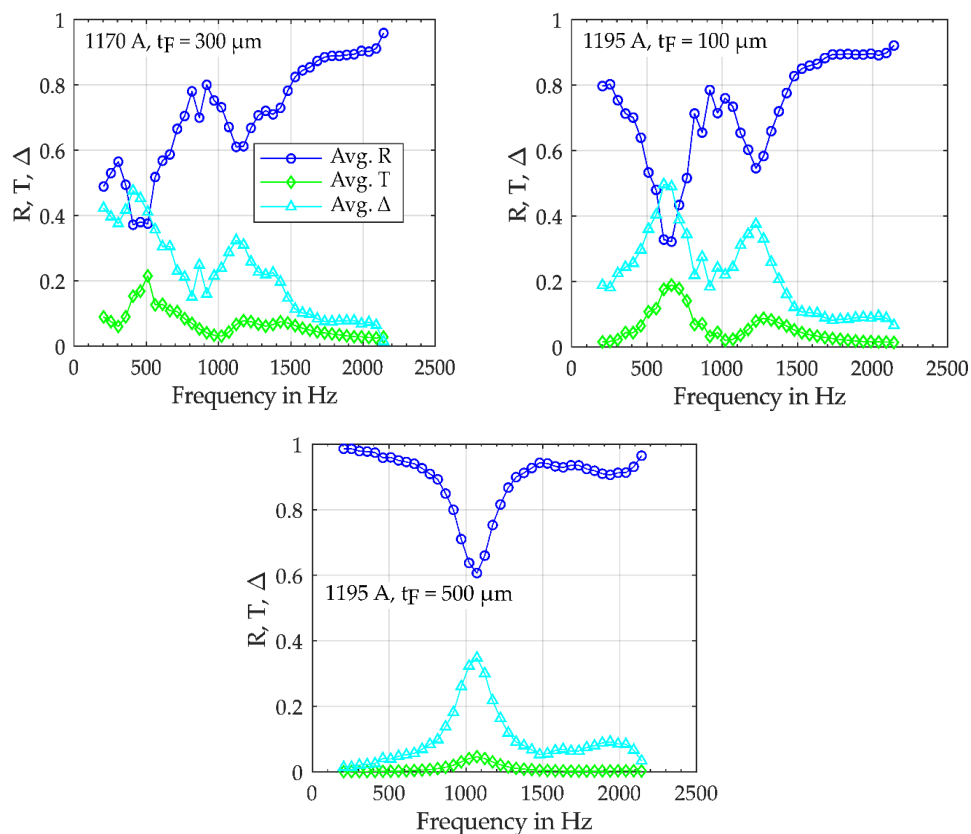


Figure 9. Vibration characteristics of flexible walls.

Comparing the transmission and dissipation curves from above figures with the dissipation curves of the complete liner assembly (see Figure 8), a coincidence of effective acoustic damping and the flexible structure vibration can be observed.

4.4. Measurement of Internal Pressure of Resonator Cells

Further insight should be gained by the installation of three microphones flush with the lower cell wall in three consecutive cells. Two examples are shown in Figure 10.

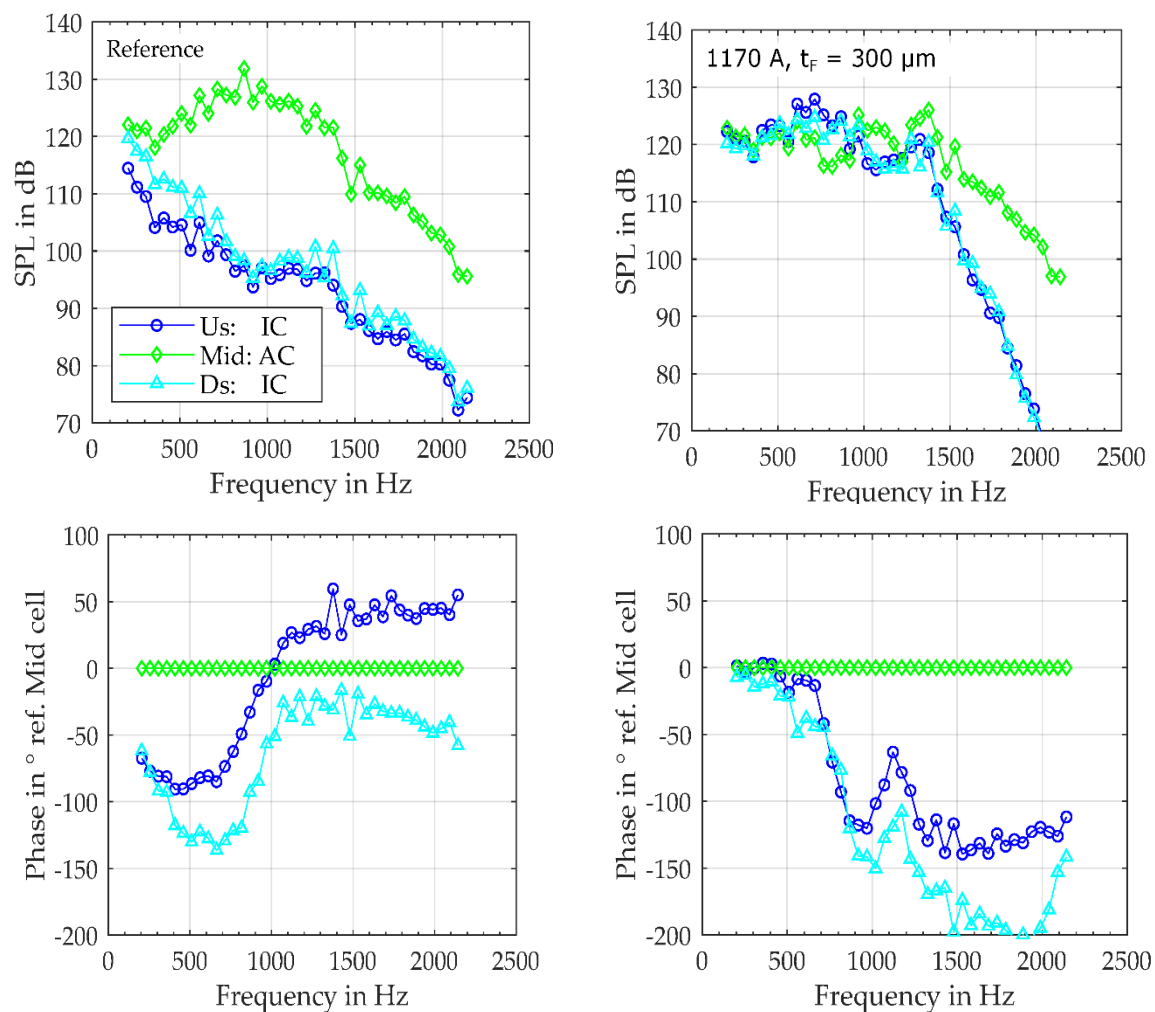


Figure 10. SPL values (**upper row**) and phase information referenced to the middle cell (**lower row**) for the reference sample (**left**) and FlexiS liner with TPU1170-0.3 (**right**); (acronyms: Us—upstream, Mid—midstream, Ds—downstream, AC—active cell, IC—inactive cell).

Here, the upstream and downstream cells were inactive, exhibiting only a small pinhole for ventilation of mean pressure in the surface. The middle cell was an active cell.

For the reference liner with rigid walls, the sound pressure in the active mid cell was much higher than for the neighbouring inactive cells over the entire frequency range. The small differences below 800 Hz might be owed to non-symmetrical pinholes in the upstream (Us) and downstream (Ds) cells. The phase difference for upstream and downstream cells coincide for a frequency of 204 Hz. Using a simple one-dimensional acoustic network model and assuming a pinhole of 0.5 mm diameter, and taking the further geometry of face sheet and cell into account, a phase difference for an acoustic wave entering the inactive cell compared to the active middle cell of around 50° is obtained. However, this value strongly depends on the geometry of the pinhole, as it is coupled to the low frequency

resonance of the inactive cell. Above 1000 Hz, where the phase shift for the middle cell occurs, the canonical behaviour of “early arrival” of the signal at the upstream cell and “late arrival” at the downstream cell can be observed, meaning that the higher frequencies can enter the cell via the pinhole, although, as visible from the SPL plot, strongly damped. For the reference liner, there is no interaction between neighbouring cells across the cell walls.

For the FlexiS liner, the behaviour is different. There are deviations in the SPL only for higher frequencies. That means that via a deflection of the flexible walls a high SPL is also generated in the inactive cells, only with frequencies above 1200 Hz not being able to produce significant deflections. Considering the small axial distance between neighbouring cells (20 mm from one to the next), an inactive cell will be subject to nearly simultaneous pressure increase from both neighbouring active cells, and subsequently simultaneous decrease again in the considered frequency range. Thus, the SPL in the inactive cells is mainly determined by the active cells.

It is rather difficult to interpret the phase information for this configuration in detail. For low frequencies, the direct coupling of active and inactive cells via the flexible cell walls is directly visible through the zero/low phase difference between neighbouring cells. The expected divergence for upstream and down-stream cells for higher frequencies can be well observed. Changes in the slope of the phase curve may relate to resonances in the cavity (and/or the flexible wall) which manifest in (local) dissipation maxima (compare Figure 8).

5. Structural Testing and Results

Experimental investigations included also a test of the structural behaviour of the honeycomb core structure. Compression tests were carried out at a constant cross-head speed of 0.5 mm/min by using a universal testing machine Zwick 1475 with a standard 100 kN load cell and computer-based data acquisition. Force was introduced into the specimen using one fixed flat platen and one spherical seat (self-aligning) platen (Figure 11). The only acceptable failure mode was uniform compressive failure of the sandwich core. The determination of the honeycomb sandwich panels' critical buckling loads and crushing behaviour was performed according to ASTM C365 (flatwise compressive properties of sandwich cores). Samples of square honeycombs ($n \leq 5$) with a number of 4 by 4 unit cells with different cell sizes and a cell wall thickness t_w of 0.5 mm were tested (Table 4). In the following \bar{x} is the mean or average (estimate of mean) and S is the standard deviation of a sample population for the given property. The walls were made of aluminium sheets with a density of 2.68 g/cm³, a Poisson's ratio of 0.33 and Young modulus of 70.5 MPa. For all specimen the cell height was adapted to ensure an equal volume of the enclosed cavity $V_c = 10.8 \text{ cm}^3$ to maintain a constant Helmholtz resonance.

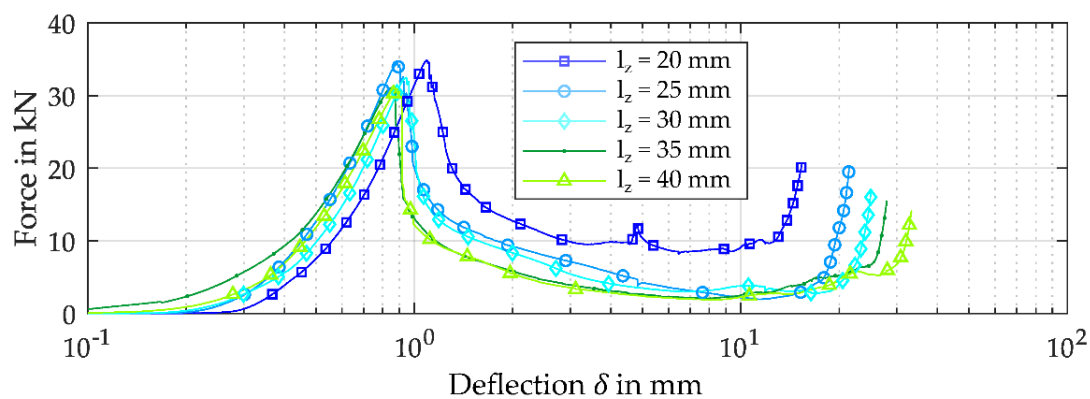


Figure 11. (a) Specimen ($B/H = 0.63$) for investigation of deformation behaviour; (b) buckling failure of honeycomb core structure.

Table 4. Results of compression tests of honeycomb core structure.

l_z	mm	40	35	30	25	20
$l_x = l_y$	mm	16.5	17.6	19	20.8	23.3
δ_{max}	mm	1.01	0.92	1.02	0.95	0.96
S_δ	mm	0.12 (12.5%)	0.14 (15.1%)	0.25 (24.7%)	0.18 (18.8%)	0.08 (8.2%)
$\bar{F}_z^{f_{cu}}$	MPa	3.79	3.6	3.12	2.86	2.34
S_F	MPa	0.14 (3.9%)	0.09 (2.6%)	0.28 (8.9%)	0.06 (2.3%)	0.06 (2.5%)

The compression tests showed a linear increase of the applied force up to the ultimate force prior to failure P_{max} . After exceeding a critical deflection δ_{max} (Figure 12), an instable buckling failure follows (Figure 11b) which leads to a rapid decrease of compression force and plastic deformation of the damaged structure. For all specimens there was no compressive failure confined to one corner or edge of the specimen. The ultimate flatwise compressive strength is defined as $F_z^{f_{cu}} = P_{max} / A_{Samp}$, where A_{Samp} is the total cross-sectional area of the honeycomb sample. The resulting δ_{max} did not show a constant trend, whereas the compression strength increases with increasing cell height. The critical deflection shows much higher deviations than the compression strength. After Buckling, starting from a relative traverse path of approximately 80%, an increase of the applied force can be seen due to a compacting of the honeycomb.

**Figure 12.** Deformation of honeycomb core structure samples under compression load.

6. Discussion

6.1. Acoustical Aspects

The measurements in the flow duct have clearly shown the additional effect of the flexible cell structure with respect to the acoustic absorption of the novel liner structure. Additional measurements—firstly, of the isolated structure with cut-outs and flexible films and secondly, the in-cell-microphone results—have proven the involved movement of the flexible wall material. However, so far little is known about the actual deflection (e.g., spatial modes) of the flexible walls. There are several main research questions, which still have to be answered:

- What is the optimum frequency for the excitation of the movement of the flexible wall? To answer this question, several efforts are required to obtain a profound description of the physical mechanism, which finally enables a precise design of the novel structures and the prediction of its performance. For the current design, it was aimed for eigenfrequencies of the flexible wall near the Helmholtz resonance of the cavity structure.
- How can the attached flexible film material be modelled? How reproducible is the assembly? Dedicated experiments measuring the spatial distribution of the actual displacement might be needed to answer these questions and model the flexible elements.

- How can the overall liner design be optimized? Currently, the inactive cells reduce the overall active liner area. What is the optimal size for the inactive cavities and can different inactive cells be coupled?

The above questions cover only a small part of possible future research on the acoustical aspects of this novel liner configuration. However, answers to these questions are mandatory in order to understand the actual mechanisms involved and model the acoustic performance at least to a certain degree of accuracy.

The effect of mean flow on the acoustic damping performance has not been shown in the current paper. However, measurements have been made with the existing samples. The observed behaviour coincides with the well-known phenomena for SDOF liners: a reduction of performance in mean flow and an increase in performance against the mean flow direction. Furthermore, it can be assumed that means to reduce non-linear effects of the face sheet resistance under grazing flow conditions, e.g., a fine wire mesh covering the face sheet of the liner, will also be applicable to the novel liner concept.

6.2. Effect of Manufacturing Related Parameters and Structure-Dynamic Aspects

There are different reasons for the discrepancy between the calculated and measured vibration behaviour. As mentioned before, manufacturing related parameter, as thickness variance, the realistic boundary conditions, the value and direction of pre-stress and relaxation effects influence the resulting resonance behaviour. The clamping of the film has to be considered as a compliant boundary; however the determination of the elasticity and damping of the adhesive bonding is difficult. Other important aspects are temperature and frequency dependent material properties of the films, as well as the influence of moisture absorption on the resulting vibration behaviour. The used material properties are gained by measurements of injection moulded samples using granulate which is pre-dried prior to processing [30]. Before testing, specimens are conditioned, thus the values of material testing can differ from the properties of finished parts. Further factors affect the physical properties, such as varying processing conditions, orientation of macromolecules and fillers, internal stresses, moisture, annealing and environmental conditions [30]. Consequently, the applied film should be tested inside the cavities during application.

For the application as an acoustic liner in aero engines the resulting mass of the honeycomb core needs to be decreased. Compared to conventional HR-Liner with rigid walls the usage of flexible walls reduces the mechanical compression resistance and enhances the risk of a stability failure. The results of the compression test show deviations due to tolerances during manufacturing, as well as levelling of the core during compression testing. A promising approach, a design with different wall thicknesses, as well as the usage of alternative manufacturing technologies could be chosen.

6.3. System Design Evaluation and Future Challenges during Development Process

Integrated into an aero engine, acoustic liners have to satisfy different jet aircraft requirements. They must be reliable and effective over a wide range of operating conditions and frequencies. Acoustic liners have to reduce broadband aero-engine noise, obtain structural strength and must have a lightweight design. In addition, they have to be adaptable to restricted available space inside the aero engine structure (liner depth and area), feature low flammability and must be cost efficient. Moreover acoustic liner structures have to satisfy manufacturability and maintainability requirements. And at the same time they have to withstand, for decades of in-service life, the aero engine environment and conditions, e.g., rain, ice, oil leaks and walking-on by maintenance personnel. Furthermore, acoustic liners must have a robust and simple design, which can be adapted and specified after the details of the airframe and engine design have been finalised.

For the implementation in the nacelle of the aero engine an assessment of the acoustic liners' system requirements and safety aspects is required. The results of the preliminary system safety assessment (PSSA), including an integrative concept study, back up the high potential of the broadband acoustic liners. Detailed information can be found in literature, e.g., [32,33]. In the following,

some of the most important points are addressed which are essential for further development and the exploitation of the full potential for a safe integration into the aircraft engines. The main aspects are:

- (a) maintaining stability despite cross-section-reduced core structures,
- (b) preservation of foil properties over the entire life cycle of the aero engine,
- (c) possibility of draining fluids and particles of dirt, and
- (d) influencing sound reflections and vibration excitation on and by adjacent systems.

By reducing the load bearing wall cross-sections, surrounding structures are subjected to enlarged stress levels. This can increase the probability of matrix or fibre breakage, as well as the risk of delamination of the top layer and general structural deformations. As a result of such fractures and deformations, the loss of the integrity of the system in flight operations or an unfavourable aerodynamic flow impairment of adjacent systems can have devastating consequences [34]. By suitable optimisation of the cut-outs in the honeycomb walls, the load-bearing capacity of the cross-section-reduced wall areas can be adapted to the respective loads [35,36]. A stress reduction in the core can be achieved by a purposeful orientation of the fibre direction in the face sheets, e.g., parallel to the walls with cut-outs.

The damping properties of the integrated film materials in the liner structure were demonstrated in this study. Nevertheless, in order to maintain noise reduction functionality and aviation safety, the behaviour of the film materials must be investigated over a longer period of time. The demands on the in-service lifetime of current acoustic liners are enormous. Since they are not actively required for flight operations, acoustic liners must be designed for the entire in-service lifetime of the engine of approximately 20 to 30 years [37]. All environmental and operating influences, as well as mechanical, chemical and aerodynamic loads must be borne by the liner structure and the integrated film materials throughout their entire in-service lifetime. No significant deterioration of the structural and noise-reducing properties shall occur within this period. Depending on the flight phase and the position in the aero engine, the occurring failure mode can have a more or less dangerous influence on flight operations.

Through targeted drainage openings in the honeycomb core, current acoustic liners are able to rinse out liquids and dirt particles that penetrate through the perforated face sheet. Honeycomb chambers which are not able to drain would collect water, dirt and other chemicals inside. This would subject the inner core structure to chemical stress [38]. At low temperatures, the fluids inside could freeze, expand and damage the liner structures and films accordingly. An impairment of the structural behaviour and mechanical properties of the rigid liner structures can also be accompanied by a reduction of the in-service life of the acoustic liner or a significant disturbance of adjacent systems. A suitable integration of drainage solutions into the broadband effective acoustic liners has to be analysed in further studies.

The vibration loads in aircraft engines can vary depending on the position of the system in the aircraft engine [37]. Accordingly, the excitation of the film structures by vibrations of adjacent systems and subsystems must be considered during the design phase. In order to fully exploit the broadband noise damping characteristics provided by the flexible film structures (also in different flight phases), an appropriate adaptation of the film dimensioning and the film's mechanical properties is indispensable. Likewise, there must be taken care not to negatively influence the adjacent systems by the vibration excitation of the acoustic liner. In addition, there is the possibility that sound reflections from the liner surface overlap with the sound waves of adjacent systems [37]. The resulting sound characteristics could lie outside the effective damping design range of the acoustic liners. An increased background noise and a higher excitation of other adjacent systems would be the result. To counteract this, the sound emission of adjacent systems should be included in the design process of the acoustic liners with flexible structures.

7. Conclusions and Outlook

The integration of highly damping polymer films as flexible walls within the cavities of Helmholtz resonators exhibits a high potential to improve the damping performance of the acoustic liner. Especially, a design with alternating active and inactive resonator cells results in additional acoustic-structural interaction of the flexible walls and yields a more broadband damping performance. The strip slotting method was used as a manufacturing technology for the square honeycomb core structure, because it enables a simple and reproducible manufacture of different flexible wall structures for the acoustic liner. Using this approach different geometrically identical acoustic liner samples were built and experimentally analysed. The acoustic-structure interaction was verified by measuring the sound pressure level in neighbouring active and inactive cells. On the one hand, the damping is influenced by the Helmholtz resonance, defined by the cavities' geometry and on the other hand by the film's structure dynamics. Therefore, the viscoelastic and physical properties as well as the film's dimensions affect the resulting acoustical behaviour. In this study thermoplastic polyurethane was analysed as a promising material due to its high damping performance and acoustically excitable elastic properties.

For application in new aero-engine nacelles, a reduction of mass in relation to the tested specimen, an adaption of the core structure's strength and the fulfilment of the comprehensive aircraft requirements is necessary. Further investigations on the description of the influencing factors, such as the arrangement and dimensions of active and inactive resonator cells, dimensioning of pressure compensation holes or the optimal film material and film size are required. However, this study shows the relevance and potential of this novel acoustic liner concept with flexible walls (FlexiS liner)—not only for aero engines, but in the entire field of sound absorbers.

Author Contributions: The individual contributions can be specified as following: Conceptualisation and supervision: M.D. and N.M.; Methodology, structural design and conduction of the manufacturing: E.K. and M.K.; Mechanical characterisation and analysis: M.K.; Acoustical design and investigations: K.K., L.E. and E.S.; Preliminary safety analysis: K.H.; Writing-Review & Editing: M.K., E.K. and M.D.

Funding: This study was financially supported by the German Federal Ministry for Economic Affairs and Energy (Luftfahrtforschungsprogramm V) within the framework of LAKS ("Lärmabsorbierende Kunststoffstrukturen") project under grant agreement no. 20E1502.

Acknowledgments: We thank our colleagues from LAKS consortium who provided insight and expertise that greatly assisted the research.

Conflicts of Interest: The authors declare no conflict of interest.

References

1. Ruijgrok, G.J.J. Attenuation of sound in duct. In *Elements of Aviation Acoustics*, 1st ed.; Delft University Press: Den Haag, The Netherlands, 1993; ISBN 90-6275-899-1.
2. Smit, M.J.T. *Cambridge Aerospace Series, Book 3: Aircraft Noise*; Cambridge University Press: Cambridge, UK, 2004; ISBN 9780521616997.
3. Follet, J.I.; Betts, J.F.; Kelly, J.J. Improvements to acoustic liner broadband absorption using bias flow. In Proceedings of the 39th Aerospace Sciences Meeting and Exhibit, Aerospace Sciences Meetings, Reno, NV, USA, 8–11 January 2001.
4. Zhao, D.; Li, X.Y. A review of acoustic dampers applied to combustion chambers in aerospace industry. *Prog. Aerosp. Sci.* **2015**, *74*, 114–130. [[CrossRef](#)]
5. Estève, S.J.; Johnson, M.E. Adaptive Helmholtz resonators and passive vibration absorbers for cylinder interior noise control. *J. Sound Vib.* **2005**, *288*, 1105–1130. [[CrossRef](#)]
6. Nagaya, K.; Hano, Y.; Suda, A. Silencer consisting of two-stage Helmholtz resonators with auto-tuning control. *J. Acoust. Soc. Am.* **2001**, *110*, 289–295. [[CrossRef](#)]
7. Zhao, D.; Morgans, A.S. Tuned passive control of combustion instabilities using multiple Helmholtz resonators. *J. Sound Vib.* **2009**, *320*, 744–757. [[CrossRef](#)]

8. Matsuhisa, H.; Ren, B.; Sato, S. Semiactive control of duct noise by a volume-variable resonator. *JSME Int. J.* **1992**, *35*, 223–228. [[CrossRef](#)]
9. de Bedout, J.M.; Franchek, M.A.; Bernhard, R.J.; Mongeau, L. Adaptive-passive noise control with self-tuning Helmholtz resonators. *J. Sound Vib.* **1997**, *202*, 109–123. [[CrossRef](#)]
10. Yamanaka, S.; Meada, F.; Shioda, K.; Iwabuchi, K.; Tsuchiya, T.; Okamoto, M. Application of Helmholtz resonators for reducing the combustion oscillation in a gas turbine. In Proceedings of the International Gas Turbine Congress 2003, Tokyo, Japan, 2–7 November 2003.
11. Liu, F.; Horowitz, S.; Cattafesta, L.; Sheplak, M. Optimisation of an electromechanical Helmholtz resonator. In Proceedings of the 12th AIAA/CEAS Aeroacoustics Conference, Cambridge, MA, USA, 8–10 May 2006.
12. Horowitz, S.; Nishida, T.; Cattafesta, L.; Sheplak, M. Characterisation of compliant-backplate Helmholtz resonators for an electromechanical acoustic liner. *Int. J. Aeroacoust.* **2002**, *1*, 183–205. [[CrossRef](#)]
13. Zaikin, A.A.; Rudenko, O.V. A nonlinear model of the Helmholtz resonator with a movable wall. *Acoust. Phys.* **1996**, *42*, 329–333.
14. Knobloch, K.; Enghardt, L.; Bake, F. Helmholtz resonator liner with flexible walls. In Proceedings of the 2018 AIAA/CEAS Aeroacoustics Conference, Atlanta, GA, USA, 25–29 June 2018.
15. Höschler, K.; Sarradj, E.; Modler, N.; Enghardt, L. Novel jet engine acoustic liner with improved broadband noise absorption. In Proceedings of the 31st Congress of the International Council of the Aeronautical Sciences, Belo Horizonte, Brazil, 9–14 September 2018.
16. Ford, R.D.; McCormick, M.A. Panel sound absorbers. *J. Sound Vib.* **1969**, *10*, 411–423. [[CrossRef](#)]
17. Kisler, R.; Sarradj, E. Plate silencers for broadband low frequency sound attenuation. *Acta Acust. United Acust.* **2018**, *104*, 521–527. [[CrossRef](#)]
18. Bitzer, T. *Honeycomb Technology: Materials, Design, Manufacturing, Applications and Testing*, 1st ed.; Springer: Dublin, CA, USA, 1997; pp. 10–22, ISBN 978-94-010-6474-3.
19. Bitzer, T. Honeycomb Marine Applications. *J. Reinf. Plast. Compos.* **1994**, *13*, 355–360. [[CrossRef](#)]
20. Geng, D.; Yi, K.; Shang, C.; Yang, J.; He, Y. Application status of composite acoustic liner in aero-engine. In Proceedings of the 10th International Conference on Composite Science and Technology, Lisboa, Portugal, 2–4 September 2015.
21. McAlpine, A.; Wright, M.C.M. Acoustic scattering by a spliced turbofan inlet duct liner at supersonic fan speeds. *J. Sound Vib.* **2006**, *292*, 911–934. [[CrossRef](#)]
22. Wadley, H.N. Multifunctional periodic cellular metals. *Philos. Trans. A Math Phys. Eng. Sci.* **2006**, *364*, 31–68. [[CrossRef](#)] [[PubMed](#)]
23. Wadley, H.N.G.; Fleck, N.A.; Evans, A.G. Fabrication and structural performance of periodic cellular metal sandwich structures. *Compos. Sci. Technol.* **2003**, *63*, 2331–2343. [[CrossRef](#)]
24. Seemann, R.; Krause, D. Numerical Modelling of Nomex honeycomb sandwich cores at meso-scale level. *Compos. Struct.* **2017**, *159*, 702–718. [[CrossRef](#)]
25. Dharmasena, K.P.; Wadley, H.N.G.; Xue, Z.; Hutchinson, J.W. Mechanical response of metallic honeycomb sandwich panel structures to high-intensity dynamic loading. *Int. J. Impact Eng.* **2008**, *35*, 1063–1074. [[CrossRef](#)]
26. BASF SE. Material Data Sheet: Thermoplastic Polyurethane Elastomers (TPU) Elastollan®—Product Range. Available online: http://www.polyurethanes.basf.de/pu/solutions/en/function/conversions:/publish/content/group/Arbeitsgebiete_und_Produnkte/Thermoplastische_Spezialelastomere/Infomaterial/elastollan_material_uk.pdf (accessed on 1 September 2018).
27. Hinrichs, C. (BASF Polyurethanes GmbH, Lemförde, Germany). Personal communication, 2018.
28. Base Engineering and Software GmbH, CAMPUS 5.2. Material Data Sheet: Elastollan®1195 A from BASF Polyurethanes GmbH. Available online: <https://www.campusplastics.com/campus/de/datasheet/Elastollan%C2%AE+1195+A/BASF+Polyurethanes+GmbH/59/b5a54956> (accessed on 22 March 2016).
29. Qi, H.J.; Boyce, M.C. Stress-strain behavior of thermoplastic polyurethanes. *Mech. Mater.* **2005**, *37*, 817–839. [[CrossRef](#)]
30. BASF SE. Material Data Sheet. Thermoplastic Polyurethane Elastomers (TPU) Elastollan®—Material Properties. Available online: http://www.polyurethanes.basf.com/pu/solutions/en/function/conversions:/publish/content/group/News_und_Medien/Spezialelastomere/Thermoplastische_Polyurethane_Elastomers_Product_Range_EN.pdf (accessed on 1 September 2018).
31. Blokhintsev, D.I. *Acoustics of a Nonhomogeneous Moving Medium*, 1st ed.; NACA Technical Memorandum 1399; National Advisory Committee for Aeronautics: Washington, DC, USA, 1956.

32. European Aviation Safety Agency. *Certification Specification and Acceptable Means of Compliance for Large Aeroplanes (CS-25)*, 20th ed.; European Aviation Safety Agency: Cologne, Germany, 2017.
33. Lloyd, E.; Tye, W. *Systematic Safety: Safety of Aircraft Systems*, 1st ed.; Civil Aviation Authority: Cheltenham, UK, 1982; ISBN 978-0860391418.
34. Kritzinger, D. *Aircraft System Safety—Assessments for Initial Airworthiness Certification*, 1st ed.; Woodhead Publishing: Cambridge, UK, 2016; Volume 33, pp. 43–44. ISBN 978-0-08-100889-8.
35. Rinker, M.; Krueger, R.; Ratcliffe, J. *Analysis of an Aircraft Honeycomb Sandwich Panel with Circular Face Sheet/Core Disbond Subjected to Ground-Air Pressurization*, 1st ed.; NASA/CR-2013-217974; National Institute of Aerospace: Hampton, VA, USA, 2013.
36. Leone, F.A.; Bakuckas, J.G.; Shyprykevich, P.; Davis, C. *Structural Testing and Analysis of Honeycomb Sandwich Composite Fuselage Panels*, 1st ed.; DOT/FAA/AR-08/51; Federal Aviation Administration: Washington, DC, USA, 2008.
37. Bräunling, W.J.G. *Flugzeugtriebwerke—Grundlagen, Aero-Thermodynamik, Ideale und Reale Kreisprozesse, Thermische Turbomaschinen, Komponenten, Emissionen und Systeme*, 4th ed.; Springer: Berlin, Germany, 2015; pp. 498–1533. ISBN 978-3-540-76370-3.
38. Li, X.; Tabil, L.G.; Panigrahi, S. Chemical treatments of natural fiber for use in natural fiber-reinforced composites: A review. *J. Polym. Environ.* **2007**, *15*, 25–33. [[CrossRef](#)]



© 2018 by the authors. Licensee MDPI, Basel, Switzerland. This article is an open access article distributed under the terms and conditions of the Creative Commons Attribution (CC BY) license (<http://creativecommons.org/licenses/by/4.0/>).